

Internal Tide Generation in the Deep Ocean

Chris Garrett and Eric Kunze

Department of Physics and Astronomy, University of Victoria, Victoria, British Columbia V8W 2Y2; Canada

Annu. Rev. Fluid Mech. 2007. 39:57–87

The *Annual Review of Fluid Mechanics* is online at fluid.annualreviews.org

This article's doi:
10.1146/annurev.fluid.39.050905.110227

Copyright © 2007 by Annual Reviews.
All rights reserved

0066-4189/07/0115-0057\$20.00

Key Words

internal tides, ocean mixing, tidal dissipation

Abstract

Internal tides are internal gravity waves generated in stratified waters by the interaction of barotropic tidal currents with variable bottom topography. They play a role in dissipating tidal energy and lead to mixing in the deep ocean. Key dimensionless parameters governing their generation include the tidal excursion compared with the scale of the topography, the bottom slope compared with the angle at which rays of internal waves of tidal frequency propagate, and the height of the topography compared with the depth of the ocean. Recent theoretical developments for parts of this parameter space particularly relevant to the deep ocean show that most of the energy flux is associated with low modes that propagate away from the generation region. For isolated features this energy flux is not strongly dependent on the bottom slope. Intense beams of internal tidal energy are expected near “critical slopes,” bottom slopes equal to the ray slope, and lead to local mixing.

1. INTRODUCTION

The tidal rise and fall of the sea surface and the associated horizontal currents have been recognized and studied for hundreds of years (Cartwright 1999). They are important for navigation, generate turbulent mixing near the seafloor, and interact with other oceanic flows and processes. The vertical movement of the ocean surface, typically of the order of a meter, is mainly associated with barotropic tidal currents. These are uniform with depth apart from a reduction near the seafloor by bottom friction, much as for water of constant density. There is, however, a small component of the surface displacement associated with motions of tidal origin in the density-stratified interior of the ocean. These baroclinic, or internal, tides have horizontal currents that are typically comparable in strength to the barotropic tidal currents, of order 0.1 ms^{-1} in the deep ocean and 1 ms^{-1} in shallow seas, but have a rich vertical structure.

Internal tides cause dramatic vertical displacements of density surfaces in the ocean interior, often several tens of meters and even hundreds of meters in some locations. These displacements, and the associated currents, complicate the mapping of the average state of the ocean, and also have major effects on acoustic transmission (Dushaw 2006), sediment transport (Cacchione et al. 2002, McPhee-Shaw 2006), and oil-drilling platforms (Osborne & Burch 1980, Osborne et al. 1978). The most important oceanographic effect of internal tides is that the vertical shear of the horizontal currents associated with them, or with other internal waves into which they transfer their energy, can be strong enough to lead to instability and turbulence. The associated mixing affects ocean structure and circulation and drives vertical fluxes of nutrients (Sandstrom & Elliott 1984).

The first recognition of internal tides is often credited to Petterson (1908). As reviewed by Hendershott (1981) and Vlasenko et al. (2005), early investigations were also motivated by Nansen's (1902) observations and led to laboratory experiments (Zeilon 1912, 1934) showing that large interfacial waves can be generated by the oscillatory flow of a two-layer fluid over bottom topography. This is easily appreciated in a frame of reference moving with the barotropic tidal current; bottom topography then acts as a wavemaker moving to and fro in the stratified fluid, not surprisingly generating internal waves.

The internal waves need not be entirely at the forcing frequencies. Strong tidal currents over topographic features with widths less than a tidal excursion can cause "lee waves," with a short wavelength, which can propagate away from the topography as high-frequency internal waves when the tide changes. Alternatively, disturbances generated at the tidal frequency can break up into short, higher-frequency motions as they propagate. These effects are common in the coastal ocean, where research into them has been conducted continuously over the past few decades (Farmer & Freeland 1983; Farmer & Smith 1980; Haury et al. 1979; Henyey & Hoering 1997; Hibiya 1986, 1988; Holloway 1987, 1996; Holloway et al. 1997; Klymak & Gregg 2004; Lamb 1994; Matsuura & Hibiya 1990; Pingree & Mardell 1985; Rippeth & Inall 2002; Sandstrom & Elliott 1984; Vlasenko et al. 1996, 2005). In the deep ocean, where the basic tidal currents are weaker, there is less likelihood of the generation of

packets of large internal waves of high frequency, so that internal tides predominantly have the same astronomically determined frequencies as the surface tide, at least near the generation sites.

The basic theory for internal tide generation in the deep sea was established several decades ago by Cox & Sandstrom (1962), Baines (1973), and Bell (1975a,b), and reviewed by Baines (1982), but since then research has been more intermittent than for shallow water. Observationally, the presence of internal tides in the deep ocean, albeit with major variations of their amplitude with time as well as in space, was recognized in current meter and other data (see Wunsch 1975 and Schott 1977 for earlier reviews), but it was thought that the energy lost to deep-ocean internal tide generation was only about 10% of the total tidal energy dissipation. This was partly because the edge of the continental shelf, which would be a powerful generator of internal tides (Rattray 1960) if the tidal elevation at the coast were supplied by tidal flows on and off the shelf, is generally not so [except in a few locations such as the Bay of Biscay (Gerkema et al. 2004, Pingree et al. 1986)] because the convergence and divergence of along-shore currents supplies most of the coastal rise and fall. It was recognized (Garrett 1979, Hendershott 1981, Wunsch 1975) that even this 10% could provide an important contribution to the mixing of the abyssal ocean, and that 10% could be an underestimate (Wunsch 1975), but the topic dropped out of fashion.

In the past decade or so this situation has changed dramatically, as summarized by Munk & Wunsch (1998) and briefly by Garrett (2003), principally with the recognition of greater importance for internal tide generation at mid-ocean topographic features. Much of this renewed interest has been inspired by the mapping of the tidal elevation of the sea surface by satellite altimetry. This has shown semidiurnal tides propagating away from mid-ocean ridges (**Figure 1**), with a wavelength that is much

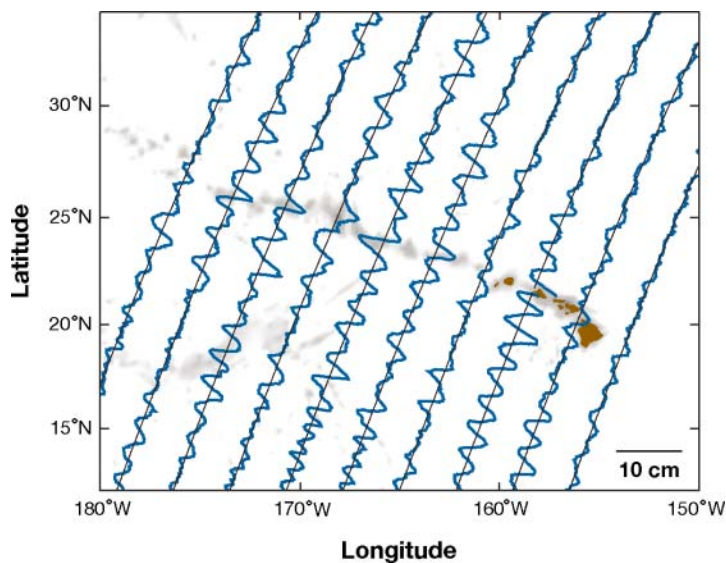


Figure 1

The amplitude near Hawaii of the surface displacement at the M_2 frequency (*blue lines* with the 10 cm scale shown), plotted normal to the TOPEX/Poseidon track (*smooth gray lines*) and high-passed with a cut-off scale of approximately 400 km. The large-scale pattern expected for the barotropic tide is alternately reinforced and reduced by motions with a much shorter wavelength (updated from Ray & Mitchum 1997, courtesy of Richard Ray, 2006).

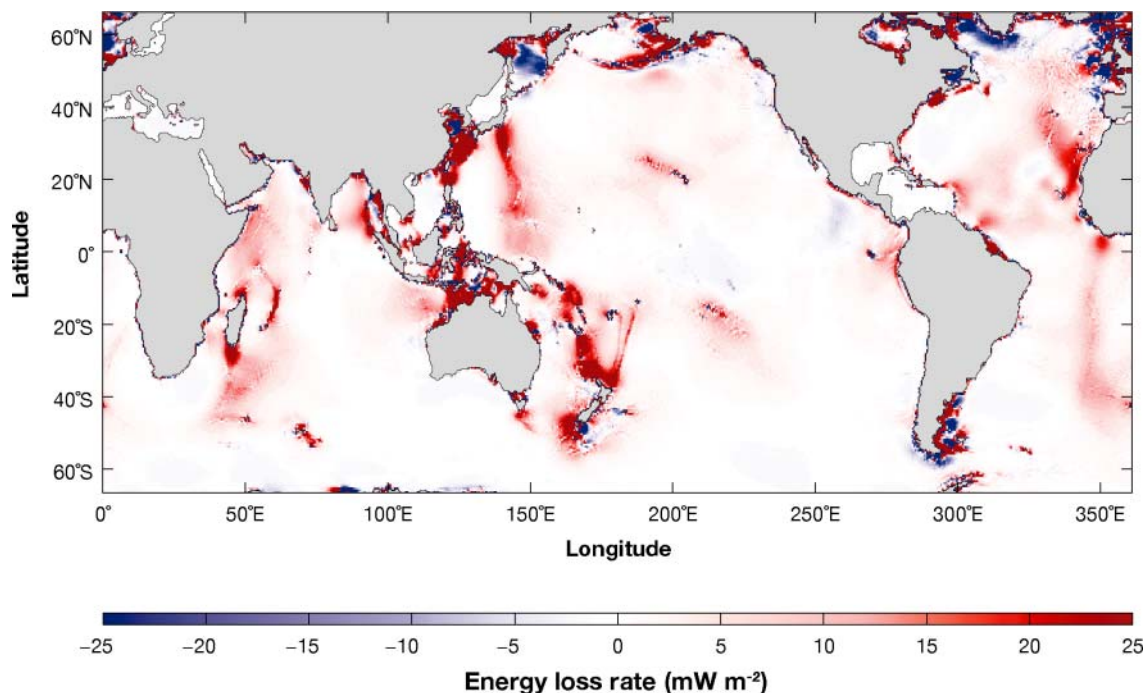


Figure 2

Estimated rate of loss of energy from the barotropic M_2 tide (Egbert & Ray 2001).

too short to match the barotropic tides but is appropriate for mode-one or mode-two internal tides (Kantha & Tierney 1997, Ray & Mitchum 1997).

On the global scale, mapping the tidal surface elevation throughout the world's oceans has led to a refined estimate of the total rate of tidal energy dissipation (Egbert & Ray 2000, 2001). This is 2.5 TW ($1 \text{ TW} = 10^{12} \text{ W}$) for the principal lunar semidiurnal tide M_2 , 3.2 TW for all lunar tides, and 3.7 TW if solar tides are included. Less than 0.2 TW of this total is dissipated in the atmosphere and solid earth (Egbert & Ray 2001). Assimilation of the altimeter data into numerical models of the surface tides (Egbert & Ray 2001) showed that they lose much more energy in the open ocean than can be ascribed to bottom friction, generally in regions with significant topographic features (**Figure 2**). The energy loss to internal tides is now thought to be 30% of the total (admittedly not hugely more than the 10% of a larger estimate for the total dissipation some decades ago). There is a feedback process: dissipation of tidal energy via internal tides plays a role in determining the magnitude of the global barotropic tides and hence affects internal tide generation.

Another reason for the revival of interest in internal tides comes from moored current meter data showing that powerful internal tide generation occurs at mid-ocean ridges (Morozov 1995). Further extensive observational programs have been initiated in recent years (Althaus et al. 2003, Rudnick et al. 2003) to examine in detail

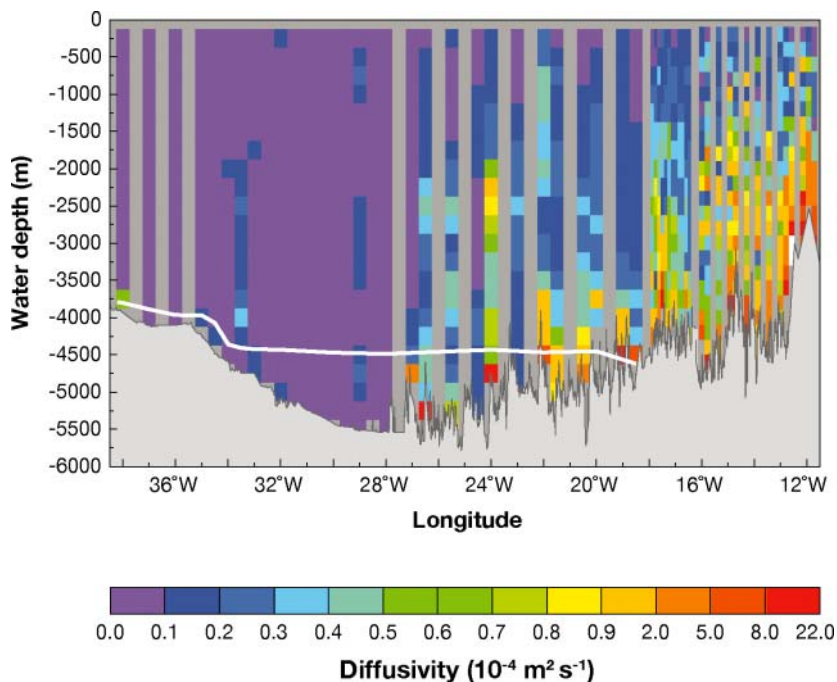


Figure 3

A section of vertical diffusivity across the Brazil Basin (Toole et al. 1997). The dark gray areas in the vertical columns indicate no data. The light area at the bottom indicates the seafloor topography. The white line shows the 0.8° isotherm.

how much of the energy transferred to internal tides is lost locally and how much radiates away.

This renewed interest in deep-ocean internal tides has coincided with increasing recognition of the dependence of the ocean's thermohaline circulation on the magnitude and distribution of mixing (e.g., Samelson 1998, Wunsch & Ferrari 2004, Zhang et al. 1999). Internal waves generated at the sea surface contribute to this mixing, as do low-frequency eddies in conjunction with air-sea interaction (Radko & Marshall 2004). However, at least for the abyssal ocean below 2 or 3 km, internal tides seem to play a role, either by leading directly to shear instability and turbulence, or by feeding energy via nonlinear interactions into smaller-scale internal waves which then break (MacKinnon & Winters 2005, Polzin 2004, St. Laurent & Garrett 2002). **Figure 3** shows a graphic illustration of this. Turbulent mixing in the abyssal Brazil Basin is much stronger near the seafloor over rough topography. This is partly because the weak stratification in the deep ocean means that little energy is required there to cause significant mixing; the turbulent energy dissipation rate and associated buoyancy flux tend to be surface-intensified. The dissipation may be modulated over the spring-neap tidal cycle (Ledwell et al. 2000), suggesting that the source of the mixing is internal tides rather than wind-generated motions propagating downward from the surface or scattered off the bottom features.

All these developments have spurred the application and extensions of earlier theoretical studies to deal with internal tide generation by the two classes of bottom topography found by Egbert & Ray (2001) to be associated with the open-ocean loss

of energy from the surface tide. These classes are (a) small but widespread roughness associated with fracture zones, and (b) tall, steep, mid-ocean ridges and island chains. Recent theoretical investigations form the main topic of this review, although we also discuss briefly some major recent field studies. Results from investigations of the different regions of parameter space relevant to the coastal ocean are beyond the scope of this review and are mentioned only briefly.

2. SETTING AND PARAMETER SPACE

The height of topographic features compared with the depth of the ocean is clearly an important factor in considering internal tide generation by some mid-ocean ridges. We consider the importance of this below. On the other hand, much of the bottom roughness in the ocean is small compared with the ocean depth, so that bottom-generated internal tides might evolve and dissipate before reflecting back to the seafloor from the surface. It is thus worthwhile to consider a semi-infinite ocean, which we suppose to have a variable bottom height $h(\mathbf{x})$, where \mathbf{x} is the horizontal coordinate, with the spatial average $\bar{h} = 0$. The Coriolis frequency f is assumed to be spatially uniform and we first take the ocean to have a linear vertical density gradient, characterized by a constant buoyancy frequency N , deferring to later a discussion of the effects of varying stratification.

The basic, barotropic, horizontal tidal current is taken as \mathbf{U} , independent of position but varying in time with frequency ω . As water flows over the bottom topography, it generates perturbation flows (\mathbf{u}, w) , where \mathbf{u} is the two-dimensional (2D) horizontal current and w is vertical. The flow must satisfy the boundary condition

$$w(b) = \mathbf{U} \cdot \nabla h + \mathbf{u} \cdot \nabla h \quad (1)$$

as well as equations of motion in the ocean interior.

Even this idealized problem has a rich dimensionless parameter space. There are six dimensional parameters: the frequencies ω, f, N , a measure b_0 of the topographic height, a horizontal scale that we take as k^{-1} , as for sinusoidal topography with wavenumber k , and the magnitude u_0 of the current \mathbf{U} . These lead to four dimensionless parameters. Three are conveniently taken as the frequency ratios ω/N and ω/f , and the parameter ku_0/ω representing the ratio of the tidal excursion u_0/ω to the topographic length scale.

The fourth dimensionless parameter needs to involve b_0 and could be taken as kb_0 . A more useful choice comes from analysis of the equations governing small-amplitude oscillatory motions in two dimensions. If these have a streamfunction $\text{Re}[\psi(x, z)\exp(-i\omega t)]$, then ψ satisfies the differential equation

$$\psi_{xx} - \alpha^2 \psi_{zz} = 0, \quad (2)$$

where

$$\alpha = \left(\frac{\omega^2 - f^2}{N^2 - \omega^2} \right)^{1/2} \quad (3)$$

is the magnitude of the slope of the characteristics of the hyperbolic Equation 2. It is also the slope of particle motion and wave rays for internal waves of frequency ω ,

and gives the ratio k/m of the horizontal wavenumber k to the vertical wavenumber m . Normalizing the bottom slope by α is helpful, so we take the fourth dimensionless parameter to be

$$\epsilon = kb_0/\alpha = mb_0. \quad (4)$$

A topographic slope equal to α so that $\epsilon = 1$ is described as “critical,” with gentler slopes termed subcritical and steeper slopes supercritical.

The two frequency ratios are important mainly in that radiating internal waves are only generated if $f < \omega < N$, assuming that $f < N$. The important parameter space to be explored is then defined by the excursion parameter ku_0/ω and the steepness parameter ϵ .

3. INFINITE DEPTH, LINEAR THEORY

We start by assuming that the problem is linear, in the sense that the advective terms $\mathbf{u} \cdot \nabla \mathbf{u}$ in the momentum equation, and similar terms in the density equation, are negligible. We also start with sinusoidal bottom topography as a building block for more complicated situations.

3.1. Small Slope

We further assume that the slope parameter ϵ is small. As is confirmed below, this allows us to neglect the term $\mathbf{u} \cdot \nabla b$ in the bottom boundary condition (Equation 1) and to apply it at $z = 0$ rather than at $z = b$. It thus becomes simply $w(0) = \mathbf{U} \cdot \nabla b$. This is the problem solved by Bell (1975a,b) for all ku_0/ω , but we start with the situation in which $ku_0/\omega \ll 1$. This permits the neglect of the advective terms in the momentum and density equations involving $\mathbf{U} \cdot \nabla$, and the response to the boundary forcing is just internal waves in a stationary medium. For the 2D (x, z) problem with $b = b_0 \cos kx$ and $\mathbf{U} = (u_0 \cos \omega t, 0)$, the response is

$$w = -kb_0u_0 \sin kx \cos(mz + \omega t), \quad (5)$$

representing waves propagating symmetrically in the positive and negative x directions. The vertical phase propagation is downward, giving upward energy propagation. The associated horizontal motions are given by

$$u = mb_0u_0 \cos kx \sin(mz + \omega t), \quad v = (f/\omega)mb_0u_0 \cos kx \cos(mz + \omega t). \quad (6)$$

These equations confirm that the simplification of the bottom boundary condition is justified for $\epsilon = mb_0 \ll 1$ because u is then much less than u_0 and the solution at $z = b$ is little different from that at $z = 0$.

Using standard equations for the internal wave energy density and the vertical component of the group velocity leads to an expression for the vertical energy flux

$$F = \frac{1}{4}\rho_0\omega^{-1}[(N^2 - \omega^2)(\omega^2 - f^2)]^{1/2}ku_0^2b_0^2, \quad (7)$$

where ρ_0 is a reference density.

It is interesting to compare this with the energy flux F_{lw} into lee waves that would be generated by a steady current of magnitude u_0 . This is

$$F_{lw} = \frac{1}{2} \rho_0 \left[(N^2 - k^2 u_0^2) (k^2 u_0^2 - f^2) \right]^{1/2} u_0 b_0^2, \quad (8)$$

with the requirement that $N > ku_0 > f$ in order to generate propagating waves (Gill 1982). For $N \gg ku_0 \gg f$, F_{lw} from Equation 8 is within a factor of 2 of F from Equation 7 for $N \gg \omega \gg f$, with the factor 2 being the difference in mean square currents in the two situations.

If ku_0 is outside the range of f to N , the energy flux into lee waves is zero. In the ocean, the requirement that $ku_0 > f$ typically restricts lee wave generation to topographic features with a horizontal scale of no more than $O(1)$ km, too small to lead to a significant energy flux or even to be resolved by global bathymetric data sets (Smith & Sandwell 1997). Thus internal wave generation by mean flows in the deep ocean is generally less effective than internal tide generation, particularly in the usual situation in which tidal currents exceed subinertial currents, although the lee wave flux may be significant in places such as the Southern Ocean.

3.1.1. Finite excursion. Lee wave theory is relevant to the internal tide problem for finite values of the excursion parameter ku_0/ω . In this case, the advective terms involving $\mathbf{U} \cdot \nabla$ must be retained, but we still assume that the problem is linear in the sense that terms such as $\mathbf{u} \cdot \nabla \mathbf{u}$ may be neglected. Bell (1975a,b) solved this problem using a transformation to a frame of reference moving with the (unidirectional) mean flow $U(t)$. For sinusoidal bottom topography, the energy flux now becomes

$$F = \rho_0 \sum_{n=1}^{n_N} n\omega [(N^2 - n^2\omega^2) (n^2\omega^2 - f^2)]^{1/2} k^{-1} J_n^2\left(\frac{ku_0}{\omega}\right) b_0^2, \quad (9)$$

where n_N is the largest integer less than N/ω . The successive terms in n come from motions generated with frequencies $n\omega$.

For small $\xi = ku_0/\omega$, $J_n(\xi) \simeq (\frac{1}{2}\xi)^n/n$. The term for $n = 1$ then dominates in Equation 9 and reduces to the expression in Equation 7. The term for $n = 2$, generated by the term $\mathbf{U} \cdot \nabla$ acting on the lowest-order solution, appears with frequency 2ω and depends on the curvature of the bottom topography. Similar arguments apply for higher harmonics.

Contributions from higher harmonics increase as ku_0/ω increases. When ku_0/ω becomes greater than 1, so that the particle excursion is greater than the scale of the topography, the internal waves are a succession of lee waves generated by quasi-steady flow over the topography, reinforced at successive passes if their phase is appropriate. Use of the asymptotic expression $J_n(\xi) \sim [2/(\pi\xi)]^{1/2} \cos(\xi - n\pi/2 - \pi/4)$ for $\xi \gg n$ shows that most of the flux in Equation 9 is associated with a value of n that increases as ku_0/ω increases and becomes large for $\omega \ll N$ when ku_0/N becomes greater than 1. In other words, the energy flux mainly appears in the stationary reference frame as high harmonics of the basic frequency ω , although still with wavenumber k . For $ku_0/N \gg 1$, the value of the flux is reduced by a factor proportional to $[N/(ku_0)]^3$ from that obtained using Equation 7. This reduction corresponds to the tidal current

$U(t) = u_0 \cos \omega t$, only satisfying the lee-wave-generating constraint $N > kU$ for part of the tidal cycle.

Overall, the reduction in the effectiveness of internal tide generation at large k means that, if we represent general bottom topography in terms of a Fourier expansion in horizontal wavenumber k , the shorter wavelengths, with $ku_0/N \gg 1$, are weighted by a factor k^{-2} in the energy flux. This may be compared with the factor k for larger scales with $ku_0/\omega \ll 1$. As confirmed below, internal tide generation at the rough seafloor in the deep ocean tends to come mainly from topographic scales large enough that we may assume ku_0/ω to be small. For coastal situations, the theory presented above provides some guidance, although nonlinear terms are often important.

So far we have assumed that ω is in the range between f and N , as is required for the generation of propagating internal tides with frequency ω . It is important to recognize that, even if $\omega < f$, as is true for the diurnal tides except at low latitudes, the harmonic terms in Equation 9 with $n > 1$ can still be important if ku_0/ω is not small. These contributions, generated as lee waves, can lead to significant mixing (Nakamura et al. 2000).

3.2. Conditions for Linearization

The importance of nonlinear terms may be examined by using the simple solutions obtained so far to begin to explore the parameter space defined by ϵ and ku_0/ω (Figure 4).

For a single plane internal wave $\mathbf{u} \cdot \nabla \mathbf{u} = 0$, as the continuity equation $\nabla \cdot \mathbf{u}$ implies $\mathbf{k} \cdot \mathbf{u} = 0$ and so $\mathbf{u} \cdot \nabla = 0$, but for more complex topography there is interaction between different waves. We thus take the spatial derivative to be equivalent to multiplying by the wavenumber. For the solution based on assuming both ϵ and ku_0/ω to be small, linearization only requires the product $\epsilon ku_0/\omega \ll 1$ (Balmforth et al. 2002). This is region 1 in Figure 4.

For the solution with both ϵ and ku_0/ω small, the radiated waves are prone to shear instability if the Richardson number $Ri = N^2/(\partial u/\partial z)^2$ is less than 1/4, or,

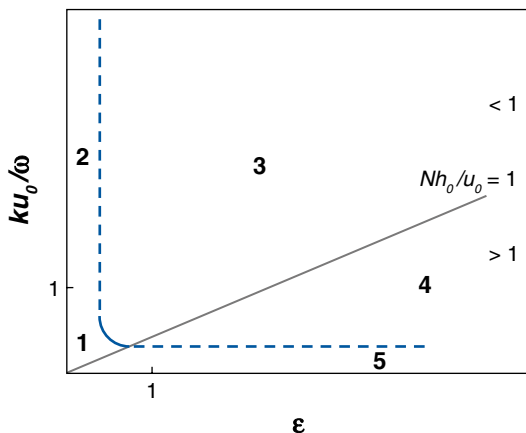


Figure 4

The parameter space defined by the steepness parameter $\epsilon = kb_0/\alpha$ and the excursion parameter ku_0/ω . The marked regions are discussed in the text. Regions with Nh_0/u_0 greater than or less than 1 are separated by the solid line with $Nh_0/u_0 = 1$.

equivalently $Ri^{-1/2} > 2$. A measure of $Ri^{-1/2}$ for the basic solution is

$$Ri^{-1/2} = A\epsilon ku_0/\omega \ll 1 \quad \text{where} \quad A = (1 - \omega^2/N^2)^{1/2}(1 - f^2/\omega^2)^{-1/2}. \quad (10)$$

Here A is typically of order 1, so that the likelihood of shear instability corresponds to the nonlinear terms becoming important. For ω close to f , A is large and the internal tide may be susceptible to shear instability within the range of validity of the linear solution.

The parameter Nb_0/u_0 is of dynamical relevance in steady, as well as oscillatory, stratified flows over topography. The influence of the stratification on the flow is minor (major) for small (large) Nb_0/u_0 . This may be written as $Nb_0/u_0 = A^{-1}\epsilon(ku_0/\omega)^{-1}$ (Legg 2004b), with a different dependence than $Ri^{-1/2}$ on ϵ and ku_0/ω . **Figure 4** shows the line corresponding to $Nb_0/u_0 = 1$. As reviewed by Baines (1995), steady flow with small Nb_0/u_0 is obtainable from linearized equations for small values of the actual steepness kb_0 ; for real fluids, flow separation is significant if kb_0 is not small. On the other hand, examination of Bell's (1975a,b) solution for region 2 of **Figure 4**, with ϵ small but ku_0/ω large, for which the internal tides are resonantly reinforced lee waves, suggests that linearization requires that $Nb_0/u_0 \ll (kb_0)^{1/3}$, a slightly stronger condition than $Nb_0/u_0 \ll 1$. On the whole, however, it seems reasonable to refer to studies of steady flow in any discussion of region 3 of **Figure 4** for which the excursion is large but Nb_0/u_0 small. This region has linear dynamics, but the bottom boundary condition cannot be linearized as it can for region 2.

For large Nb_0/u_0 in steady flow, there is a tendency for upstream blocking and nonlinear hydraulic effects (Baines 1995). We might expect these effects also to occur for oscillatory flow with finite ku_0/ω and values of Nb_0/u_0 that are not small (region 4 of **Figure 4**), as has been found in numerical models (Legg 2004b, Legg & Huijts 2006) discussed below. We note that region 4 is limited to large ϵ ; hydraulic effects and associated local mixing are unlikely for broad features with subcritical slopes.

Finally, in this superficial discussion of the parameter space of **Figure 4**, we come to region 5, with small excursion parameter ku_0/ω but finite steepness parameter ϵ . As we discuss in the next section, higher spatial harmonics are generated as ϵ increases (with a singularity at $\epsilon = 1$), although still with frequency ω if ku_0/ω is small. This contrasts with the smooth transition from region 1 to region 2 of **Figure 4**, in which higher temporal harmonics are generated as ku_0/ω increases, although all with wavenumber k .

3.3. Finite Slope

In addressing the problem with small ku_0/ω and increasing ϵ , a first step is to consider an expansion in powers of ϵ . Higher harmonics of k appear in the power series, but corrections to the energy flux in Equation 7 only involve even powers of ϵ . St. Laurent & Garrett (2002) found that, to lowest order, the flux is increased by a factor $1 + \frac{1}{4}\epsilon^2$, although there is a proportionately much larger increase in the mean square shear, as one might expect from the presence of higher spatial harmonics.

Balmforth et al. (2002) continued the power-series expansion for the correction factor, finding that it converges for any ϵ up to 1 where it reaches a value of 1.5561. Thus, the increase in energy flux is modest. Balmforth et al. (2002) confirm that

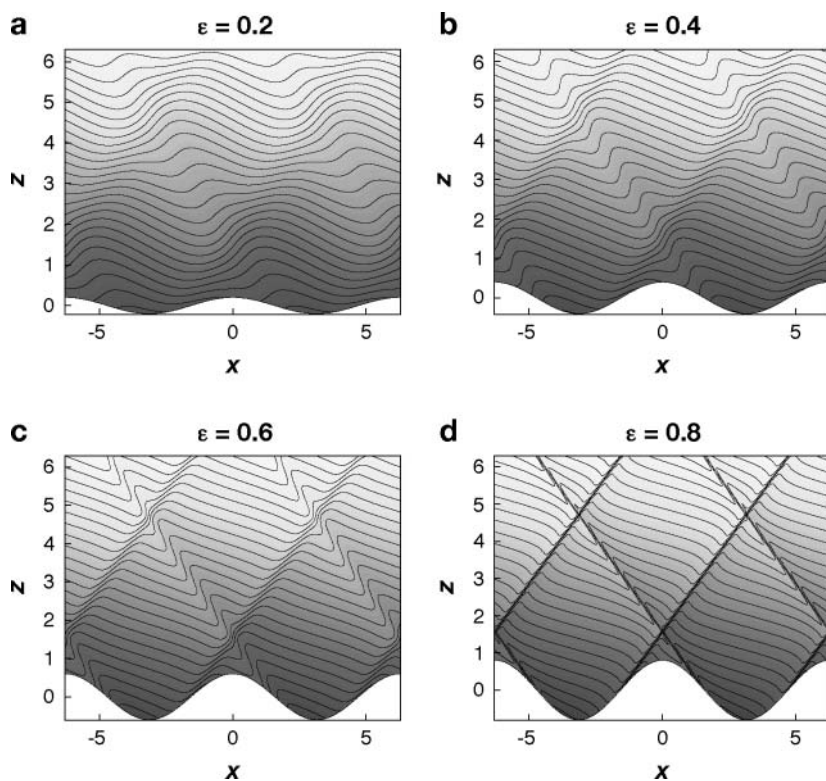


Figure 5

Snapshots of density surfaces for $\epsilon ku_0/\omega = 0.5$ and various values of ϵ (Balmforth et al. 2002). The horizontal and vertical scales are nondimensionalized such that the bottom topography has a height proportional to $\cos x$ and internal tide rays are inclined at 45° .

beams with increasingly sharp gradients appear in the solution as ϵ increases, even for fixed $\epsilon ku_0/\omega$ (Figure 5). Thus the use of $\epsilon ku_0/\omega$ as a measure of nonlinearity breaks down as ϵ increases. Overturning (as would occur for the solutions in panels c and d of Figure 5) and shear instability occur as ϵ approaches 1, even if the tidal forcing represented by ku_0/ω is very weak.

Balmforth et al. (2002) also examine the solution for other forms of topography, with ϵ based on the maximum topographic slope. As ϵ approaches 1 for an isolated Gaussian bump, the energy flux only increases by 14% from the value calculated assuming that ϵ is very small. Again, however, beams with sharp gradients appear as ϵ increases. For both the bump and sinusoidal topography (Figure 5), sharp gradients in the solution appear on internal wave rays originating from the steepest part of the topography.

3.4. Steep Topography

Any smooth topography with a maximum slope greater than critical ($b_x = \alpha$) will inevitably have some points at which the slope is critical. The results described above suggest that, in the neighborhood of such points, very sharp gradients appear in the form of beams and the linear solution is not applicable. On the other hand, the small-scale motions for which the linear solution breaks down correspond mainly to waves

that have a small group velocity and so do not carry much of the energy flux. It seems reasonable to assume that larger-scale motions, which carry most of the energy flux, are unaffected by a breakdown of the linear solution at small scales, so it is worthwhile to examine solutions for steep topography, with $\epsilon > 1$, on the assumption of linearity, while also assuming that $ku_0/\omega \ll 1$.

3.4.1. Knife edge. The limit of $\epsilon \rightarrow \infty$ corresponds to topography with vertical sides. One appealing problem has been that of a knife-edge barrier, generally in the broader context of an ocean of finite depth where, as discussed below, the solution is sensitive to the ratio of barrier height to ocean depth. If the barrier height is very small compared with the ocean depth, however, a knife edge of height b_0 leads to the generation of only twice as much energy flux as occurs in a semi-infinite ocean for a ‘‘Witch of Agnesi’’ barrier given by

$$b(x) = b_0 \left(1 + \frac{x^2}{b^2} \right)^{-1}, \quad (11)$$

after Fourier decomposition and application of the theory for $\epsilon \ll 1$. This factor of 2 was obtained numerically (St. Laurent et al. 2003), following an early formulation by Robinson (1969), and analytically (although requiring the hydrostatic assumption, equivalent to $\omega \ll N$) by Llewellyn Smith & Young (2003), who point out that it is implicit in an earlier study by Hurley (1997) in the nonrotating case. The result shows that the height of an isolated ridge in a deep ocean is the main factor determining the energy flux, without a great sensitivity to the slope of its sides.

3.4.2. Broader ridges. One obvious criticism of the knife-edge solution is that its infinitesimal width means that the parameter ku_0/ω cannot be small. However, broadening the knife edge into a top hat does not greatly affect the predicted energy flux (St. Laurent et al. 2003), although this result depends somewhat on ocean depth (see below).

Thus, as ϵ increases for a ridge of a given height but decreasing width, the internal tide energy flux increases by about 50% as $\epsilon \rightarrow 1$ (the 56% increase cited above was for a Gaussian shape, not a Witch of Agnesi) and only by 100% as ϵ approaches infinity.

The possibility remained that greater increases occur for values of ϵ between 1 and ∞ , but this was effectively laid to rest in a study of a ridge of triangular cross section and other shapes, with supercritical but finite slopes (Petrelis et al. 2006). For a ridge of a given height, there is a rapid increase in energy flux for slightly supercritical slopes, but without any intermediate maximum of the flux for ϵ between 1 and ∞ .

4. FINITE DEPTH, LINEAR THEORY

4.1. Normal Modes

In an ocean of finite depth, only topography with wavenumbers matching horizontally propagating modes can radiate internal tides (Cox & Sandstrom 1962, Khatiwala

2003, Llewellyn Smith & Young 2002). In an ocean with constant N and depth H , the lowest mode has half a wavelength in the vertical so that $mH = \pi$ and $k = \alpha\pi/H$. Features with a horizontal scale larger than $(\alpha\pi)^{-1}H$ cause forced barotropic or bottom-trapped baroclinic disturbances locally, with no radiated energy.

4.1.1. A simple ridge. This can be illustrated by considering a Witch of Agnesi profile (Equation 11) in an ocean of constant N and depth H . Assuming $ku_0/\omega \ll 1$ and $\epsilon \ll 1$, where $\epsilon = (3^{3/2}/8)(b_0/b)\alpha^{-1}$ is associated with the maximum slope of the ridge, the energy flux (St. Laurent et al. 2003, Llewellyn Smith & Young 2002) is

$$F_{\text{linear}} = F_0 \frac{\pi^2}{4} \delta^2 \sum_{n=1}^{\infty} n c^2 e^{-nc} \quad (12)$$

$$= F_0 \frac{\pi^2}{4} \delta^2 \frac{c^2 e^{-c}}{(1 - e^{-c})^2}. \quad (13)$$

Here $\delta = b_0/H$ is also small, $c = (3^{3/2}\pi/4)(\delta/\epsilon) = 2b/H$ and

$$F_0 = (2\pi)^{-1} \rho_0 \omega^{-1} [(N^2 - \omega^2)(\omega^2 - f^2)]^{1/2} u_0^2 H^2. \quad (14)$$

The index n in the summation in Equation 12 corresponds to the mode number and the exponential term comes from the Fourier transform of Equation 11. For a very deep ocean, with $c \rightarrow 0$, the sum in Equation 12 merges into the integral given by the theory for infinite depth. This limit is $F_{\text{linear}} = F_0 \pi^2 \delta^2 / 4$, independent of the width of the ridge for this particular shape (Llewellyn Smith & Young 2002). If c is not small, the energy flux decreases significantly, mainly because of the absence of energy flux from the large-scale components of the bottom topography.

4.1.2. A small step. Another interesting example (St. Laurent et al. 2003) is with

$$b(x) = \pi^{-1} b_0 \tan^{-1} \frac{x}{b}. \quad (15)$$

This is proportional to the integral of Equation 11 and represents a transition from depth $H + \frac{1}{2}b_0$ to $H - \frac{1}{2}b_0$. As before, $\delta = b_0/H$ is small and the maximum slope parameter is $\epsilon = \pi^{-1}(b_0/b)\alpha^{-1}$. The energy flux is now

$$F_{\text{linear}} = F_0 \delta^2 \sum_{n=1}^{\infty} n^{-1} e^{-4(2-\delta)^{-1}n(\delta/\epsilon)} \quad (16)$$

$$= -F_0 \delta^2 \ln \left(1 - e^{-4(2-\delta)^{-1}(\delta/\epsilon)} \right). \quad (17)$$

For a very deep ocean with $\delta/\epsilon \ll 1$, and so $\delta \ll 1$ also as ϵ is small, the energy flux becomes

$$F_{\text{linear}} = F_0 \delta^2 \ln \left(\frac{1}{2} \epsilon / \delta \right). \quad (18)$$

This still depends on the depth of the ocean because the Fourier transform of the topography is proportional to k^{-1} for small k so that there are always scales, which are too large to generate radiating modes.

4.2. Large Features

The above analyses require that both (a) the slope parameter $\epsilon \ll 1$ to permit an approximation to the bottom boundary condition, and (b) the height ratio $\delta \ll 1$ so that the barotropic current, which generates the internal tides is independent of horizontal position. Many ocean features, particularly some responsible for large loss of energy from the barotropic tide (Egbert & Ray 2001), violate one or both of these approximations so that more general approaches are required. We describe below two different formulations, but first discuss some examples of “abrupt” topography of finite height compared with the depth of the ocean, i.e., $\epsilon = \infty$ and δ not small.

4.2.1. Knife edge, step, and top hat. The knife-edge problem was referred to above in the context of an ocean of infinite depth. For an ocean of finite depth, St. Laurent et al. (2003) matched modal solutions on either side of the ridge and showed that for intermediate values of δ there is a rapid falloff of energy flux with increasing mode number. **Figure 6** shows the total internal tide energy flux, compared with that for a Witch of Agnesi profile (Equation 11), using the formula (Equation 13) from linear theory but taking $\epsilon = 1$. It has a limit, mentioned above, of 2 as $\delta \rightarrow 0$ and a rapid rise as δ approaches 1. Part of this rise is due to a falloff in the factor in Equation 13 involving c , from 1 when $\delta = 0$ to 0.3 when δ approaches 1.

Llewellyn Smith & Young (2003) used their exact solution for the knife-edge problem (albeit using the hydrostatic approximation requiring $\omega \ll N$) to express the energy flux as

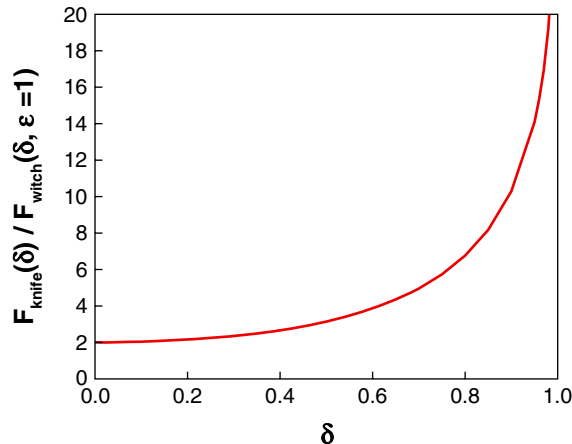
$$F_{\text{knife}} = 2\pi F_0 \int_0^\delta Y \left(\frac{1 - \cos \pi Y}{\cos \pi Y - \cos \pi \delta} \right)^{1/2} dY. \quad (19)$$

This provides an analytical confirmation of the factor of 2 compared with the Witch of Agnesi for small δ , and also shows that the flux is proportional to $-\ln(1 - \delta)$ as δ approaches 1.

St. Laurent et al. (2003) also used modal expansions to evaluate the energy flux generated by a vertical step from depth H to $H - b_0$. For small δ , the energy flux

Figure 6

The energy flux from a knife-edge ridge normalized by that given by linear theory for a Witch of Agnesi profile with $\epsilon = 1$ (St. Laurent et al. 2003).



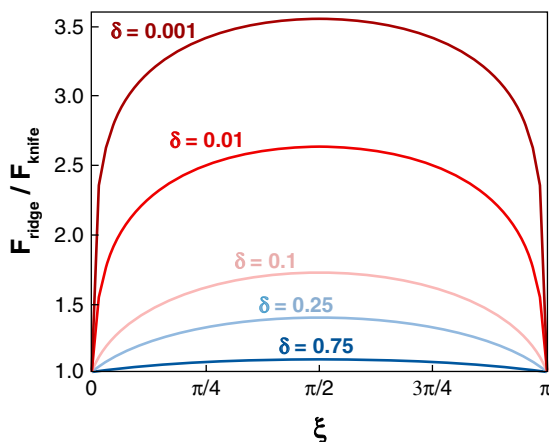


Figure 7

The energy flux from a top-hat ridge normalized by that from a knife-edge, as a function of $\chi = \alpha\pi L/(H - b_0)$ for various values of δ (St. Laurent et al. 2003).

from an abrupt step is given by the formula (Equation 18) for a gradual rise with the factor $\frac{1}{2}\epsilon/\delta$ in the logarithm replaced by $3.4/\delta$. In other words, the small step has the same effect as taking a slope factor $\epsilon = 6.8$ in the formula based on assuming $\epsilon \ll 1$.

The knife-edge and step solutions in finite depth provide for a useful comparison with the solution for a top-hat ridge (**Figure 7**). As a consequence of destructive and constructive interference, the solution for a top hat is periodic in the parameter $\chi = \alpha\pi L/(H - b_0)$, where $2L$ is the ridge width, in the sense that the radiated waves are the same for $\chi = j\pi + \phi$ for any integral value of j including zero. For ridges of any significant height compared with the depth of the ocean, the top hat generates much the same energy as a knife edge, whatever the ridge width. Only for small δ does the top hat act as two separate small steps and generate a greater flux than from a knife edge of the same height, as long as there is no destructive interference (St. Laurent et al. 2003).

St. Laurent et al. (2003) also showed that the energy flux from a top-hat trench is typically less than that from a top-hat ridge with height equal to the trench's depth, breaking the symmetry for small features found by Balmforth et al. (2002) for ϵ up to 1.

4.3. Variable Stratification

With variable stratification $N(z)$, Equation 2 still applies, but with α now also a function of z . There is no major difficulty in extending the linear theory for internal tide generation provided that the bottom topography has gentle slopes, with $\epsilon \ll 1$, and is small compared with the depth of the ocean, with $\delta \ll 1$ (Balmforth et al. 2002, Khatiwala 2003). The response is now in the normal modes for the actual stratification. For high modes, with vertical wavelength small compared with the depth of the ocean, the energy flux is close to that for an ocean of infinite depth with a constant N taken to be that at the seafloor.

Using the bottom N is also appropriate in calculating the response for small features of finite steepness, but the general problem with finite ϵ and δ , even with

$ku_0/\omega \ll 1$, is more complicated. For the knife edge, St. Laurent et al. (2003) suggested that the normalizing value of F_0 in Equation 14 should be evaluated using N at the top of the ridge and the depth ratio δ evaluated after WKB stretching of the vertical coordinate. This result is supported to within 20% by a formal analysis using a WKB expansion (Llewellyn Smith & Young 2003).

The solutions for abrupt topography provide some guidance for the energy flux expected at features with a height that is not a small fraction of ocean depth, but it is clearly necessary to have a more general approach for both small and large values of the slope parameter.

4.4. The Body Force Approach

The approximation of applying the bottom boundary condition at the average seafloor requires that $\epsilon \ll 1$ and also that $\delta \ll 1$ so that the generating barotropic flow can be taken as independent of x . Baines (1973) avoided both of these limitations by taking the basic flow as that which would occur in a homogeneous flow over the same topography. The baroclinic flows must then satisfy the condition of zero normal flow at the seafloor and are generated by an effective vertical body force in the interior of the fluid.

The equation for the vertical acceleration has a buoyancy forcing term b given by

$$\frac{\partial b}{\partial t} = -N^2 w_1, \quad (20)$$

where $N(z)$ is the buoyancy frequency of the basic state and $w_1 = -Qz(H - b)^{-2}b_x$ is the vertical velocity for hydrostatic flow in a homogeneous ocean with the sea surface at $z = 0$, the seafloor at $z = -H + b$, and a barotropic transport $Q(t)$. The governing equation (Equation 2) for the streamfunction (where the velocity components are $u = -\partial\psi/\partial z$ and $w = \partial\psi/\partial x$) now has a forcing term S on the right-hand side given by

$$S = Qz(1 - \omega^2/N^2)^{-1} \frac{d^2}{dx^2}(H - b)^{-1}. \quad (21)$$

The forcing is largest above steep topography (at least in a 2D situation in which the basic flow cannot avoid slopes).

Solving the 2D problem is complicated by the need to impose a radiation condition on the baroclinic solutions. This leads to an integral equation, with different approaches needed depending on whether the bottom slope is less than or greater than that of the internal tide rays. Numerical solutions (Gerkema et al. 2004) starting from an ocean at rest automatically satisfy the radiation condition provided that reflection from the open boundaries of a model domain is avoided through the use of sponge regions.

4.5. A Green's Function Approach

A different general approach, for 2D problems and using the hydrostatic approximation for $\omega \ll N$, was proposed by Petrelis et al. (2005). They used Robinson's (1969) Green's function, which satisfies the radiation condition, to write down the response

to an arbitrary distribution of sources and sinks on the surface of a ridge (taken to be symmetric). The condition of zero normal flow for the combined surface tide and internal tide leads to an integral equation, for the source/sink distribution, which Petrelis et al. (2005) solved numerically for a triangular ridge and a ridge of more rounded shape. Both of these reduce to a knife edge as the width tends to zero.

Their results confirm the conclusion mentioned above for an ocean of infinite depth, that there is a monotonic increase in the radiated energy flux as a ridge of a given height becomes steeper, with most of the increase happening as the maximum slope increases from critical to slightly supercritical. A knife edge is thus a good model for any isolated steep high ridge provided the excursion parameter ku_0/ω is small.

4.6. Boundary Forcing and Characteristics

Vlasenko et al. (2005) also formulate the 2D linear problem in terms of boundary, rather than interior, forcing. The governing equation is then Equation 2, with boundary conditions of $\psi = 0$ at the surface $z = 0$ and $\psi = Q$ at the bottom $z = -H + b$. We note, however, that the transformation $\psi' = \psi + Qz/(H - b)$ changes the boundary condition to $\psi' = 0$ at both top and bottom, while adding a forcing term $Qz \frac{d^2}{dz^2} (H - b)^{-1}$ to the right-hand side of Equation 2 for ψ' . This lacks the factor $(1 - \omega^2/N^2)^{-1}$ in Equation 21, showing that although the Baines (1973) equation is often assumed to be valid for nonhydrostatic conditions, it is then incorrect (Garrett & Gerkema 2006). The factor should be dropped, conveniently simplifying the problem.

With variable stratification, Vlasenko et al. (2005) first transform the problem to a coordinate frame in which the characteristics are straight. This is done by defining a new vertical coordinate

$$z_1 = \int_0^z \alpha^{-1}(\zeta) d\zeta, \quad (22)$$

where α is defined by Equation 3 with $N(z)$ and assumed real, requiring $f < \omega < N$. A scaled streamfunction $\Psi = \alpha^{-1/2} \psi$ then satisfies

$$\Psi_{xx} - \Psi_{z_1 z_1} + p(z)\Psi = 0, \quad (23)$$

where

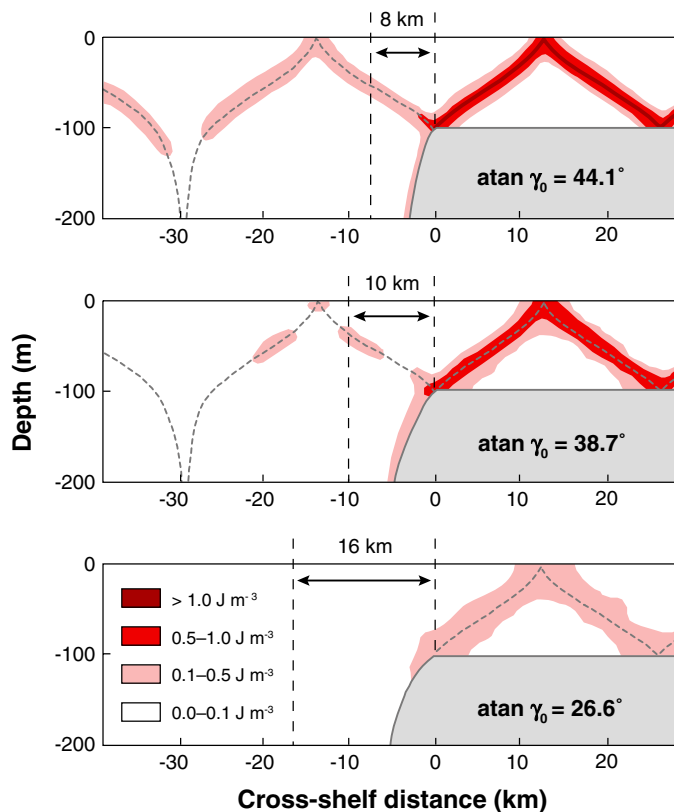
$$p(z) = \frac{1}{4} \left(\alpha_z^2 - 2\alpha\alpha_{zz} \right). \quad (24)$$

At the bottom boundary, $\Psi = \alpha^{-1/2} Q$. Vlasenko et al. (2005) show how to solve the problem using characteristics. The solution is facilitated if $p(z)$ in Equation 24 is constant, as for a particular class of $N(z)$ profiles with a maximum to represent a pycnocline. **Figure 8** shows some solutions for internal tide energy generated at a continental slope for different values of its steepness.

The solution here, as in other studies of the continental slope (Craig 1987, Gerkema et al. 2004, Prinsenberg & Rattray 1975), and as expected from studies for small-amplitude features (**Figure 5**), shows the most intense response in beams originating from regions with slopes close to that of the rays. This strong response is spatially limited and thus largely associated with large wavenumbers that have small

Figure 8

The internal tide energy density resulting from forcing at a continental slope with a steepness that is constant with respect to the scaled vertical coordinate and equal to the ray slope for arctan $\gamma_0 = 45^\circ$. The width of the continental slope is indicated by the vertical dashed lines. The barotropic tidal forcing has a current of 0.01 m s^{-1} in the deep ocean of depth 4 km, with a tidal period of 12.4 hours and latitude 30° . The stratification has a maximum N of 10^{-2} s^{-1} at a depth of 30 m, decreasing by a factor of 2 at 25 m above and below this depth (Vlasenko et al. 2005).



group speeds. Most of the energy flux is carried by low modes that have amplitudes that are much more sensitive to the height of the bathymetric feature than to its slope. In particular, Craig (1987) found little change in the energy flux generated by a continental slope once it was steeper than critical, and Gerkema et al. (2004) found that the solution for a step is reasonably accurate for any supercritical slope.

Figure 8 suggests that the motions are more intense on the shelf than in the deep sea, but solutions for a step (St. Laurent et al. 2003) and with a more detailed model (Baines 1982) show a considerably larger energy flux into the deep ocean than onto the shelf.

This is not to discount the importance of intense bottom currents near critical slopes. The associated mixing, although local, can be important, and the effect of the currents on sediment transport may even mean that continental slopes are to some extent shaped by internal tides (Cacchione et al. 2002).

4.7. Three Dimensions

Linear theory for small values of ϵ and δ is also easily extended to allow for 2D bottom topography. St. Laurent & Garrett (2002) point out that choosing coordinate axes parallel to the major and minor axes of the basic tidal current means that the internal

tides generated by the two current components are out of phase and may be treated independently; there are no cross terms in a calculation of the energy flux.

Simple 3D theoretical solutions for a wider range of parameter space are presently lacking. However, using finite difference numerical models, Holloway & Merrifield (1999) and Munroe & Lamb (2005) showed that large seamounts are ineffective at generating internal tides unless they are elongated in a direction normal to the barotropic current. In this case, the 2D models are generally applicable, but the barotropic current over the ridge is reduced by a tendency for water to flow around it, particularly if the stratification is strong so that Nh_0/u_0 is not small. More investigation is warranted of a parameter space that now includes the lateral aspect ratio of a bottom feature. Trapped subinertial waves can also be generated at seamounts by the subinertial diurnal tide (Brink 1990, Codiga & Eriksen 1997), but are not discussed here.

5. NUMERICAL MODELS OF IDEALIZED NONLINEAR SITUATIONS

Our discussion so far has covered the full range from 0 to ∞ of the two key parameters ϵ and ku_0/ω , but only if the solution is linear. As discussed above with respect to **Figure 4**, this condition is satisfied for any value of ku_0/ω provided that ϵ is small, and may be relaxed to $\epsilon ku_0/\omega \ll 1$ if both parameters are small, i.e., it allows for larger slopes if the tidal excursion is very small.

For values of ϵ near or greater than 1, there will be regions of the flow in which the assumption of linearity breaks down. We have argued that for region 5 in **Figure 4**, with $ku_0/\omega \ll 1$ but arbitrary ϵ , it is still useful to solve linearized equations as the solution will correctly describe the large-scale motions that contain most of the energy flux. Khatiwala (2003) confirmed this using a numerical model. His results show the expected large fine-scale shears, but the energy flux is not greatly changed by the nonlinearity and dissipation at small scales.

Numerical models are necessary and instructive for other regions of **Figure 4** in which simple analytical models break down (Legg 2004a,b; Legg & Huijts 2006). In particular, for along-slope flow over a corrugated continental slope (Legg 2004b), with large ku_0/ω and ϵ but $Nh_0/u_0 > 1$ (region 4 in **Figure 4**), there is significant mixing in hydraulic jumps downstream from the crests of ridges. This is as expected from studies of steady flows (Baines 1995) but, in the oscillatory case, packets of dispersive high-frequency waves are also released each tidal cycle (Legg 2004b). Numerical studies by Legg & Huijts (2006) for a Gaussian ridge confirmed the expectation that strong hydraulic effects and vigorous local mixing only occur for narrow features with large ϵ as well as significant ku_0/ω , a situation that is rare in the deep sea but common in the coastal ocean (e.g., Klymak & Gregg 2004).

5.1. Finite Depth

The situation changes if the water depth is finite or if the internal tide is trapped in a pycnocline. The effects of wave dispersion can now be balanced by the tendency for

horizontally propagating modes or interfacial waves to steepen at finite amplitude. A number of situations are possible, depending on the height ratio δ and details of the stratification as well as the two key parameters ϵ and ku_0/ω . The frequency ratios ω/N and ω/f can also have an influence. If there is a pycnocline with strong stratification, its depth with respect to the height of a ridge crest can be important. Vlasenko et al. (2005) discuss the full parameter space and a variety of numerical solutions, which are not reviewed in detail here.

As mentioned in the Introduction, even if an internal tide is generated in a linear manner, nonlinear effects can occur during its propagation; a periodic wave of tidal frequency can steepen into a “solibore” in which a propagating change of isopycnal displacement is associated with a train of short, high-frequency, finite-amplitude waves resembling solitary waves. These can occur sooner if the generation process is nonlinear; nonlinear lee waves can appear as an internal depression downstream of a ridge, propagate back across the ridge as the current slackens, and quickly break up into a solibore. Farmer & Armi (1999) found a different situation, examined further by Cummins et al. (2006), with upstream solitary waves appearing while the tidal current is increasing rather than decreasing, but it is not known how widespread this might be.

Gerkema (1996) and Gerkema & Zimmerman (1995) argued that the importance of nonlinear terms in these situations is governed by a dimensionless parameter given by $(ku_0/\omega)\delta$ using the notation of this paper. A large tidal excursion and/or a large ridge height compared with the depth of the ocean is required for significant nonlinearities. This is for an effectively two-layer situation and discounts the effects discussed above for a continuously stratified ocean, in which the steepness parameter ϵ is important.

6. SOME APPLICATIONS FOR REAL TOPOGRAPHY

6.1. Linear Analytical Models

Many areas of rough topography in the deep ocean, such as the Mid-Atlantic Ridge (**Figure 9**), have subcritical slopes and small ku_0/ω for horizontal scales larger than a few hundred meters (**Figure 10**).

Linear theory shows that the energy flux is nearly all derived from scales for which the approximations are valid, even after allowing for the finite depth of the ocean by discounting the flux from horizontal scales larger than that of the lowest mode. It thus seems reasonable to apply the simple theory in these regions of the deep ocean.

Nycander (2005) applied linear theory for small bottom slope to global bottom topography, finding a plausible flux of 1.2 TW into internal tides at the M_2 frequency, or 1.8 TW into all internal tides, but finds that about half of this comes from supercritical topography for which the model is inappropriate. This is consistent with other findings that a large fraction of the energy loss from the barotropic tide in the open ocean is associated with steep isolated features (Egbert & Ray 2001, Niwa & Hibiya 2001, Simmons et al. 2004). For these regions, however, even more than for gentle topography, the expectation from simple 2D analytical models (Llewellyn Smith & Young 2003, Petrelis et al. 2006, St. Laurent et al. 2003) is that most of the energy

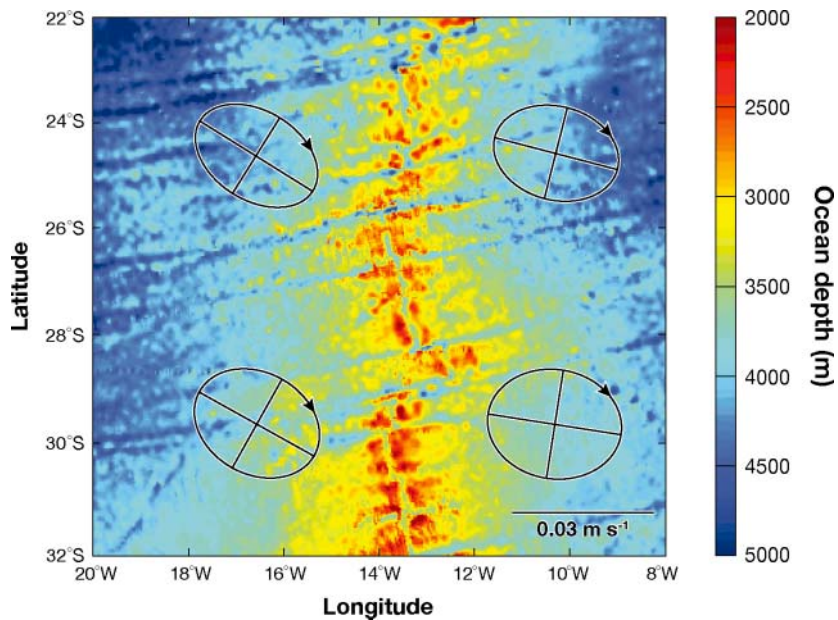


Figure 9
The bottom topography for a region of the Mid-Atlantic Ridge and local M_2 tidal ellipses (St. Laurent & Garrett 2002).

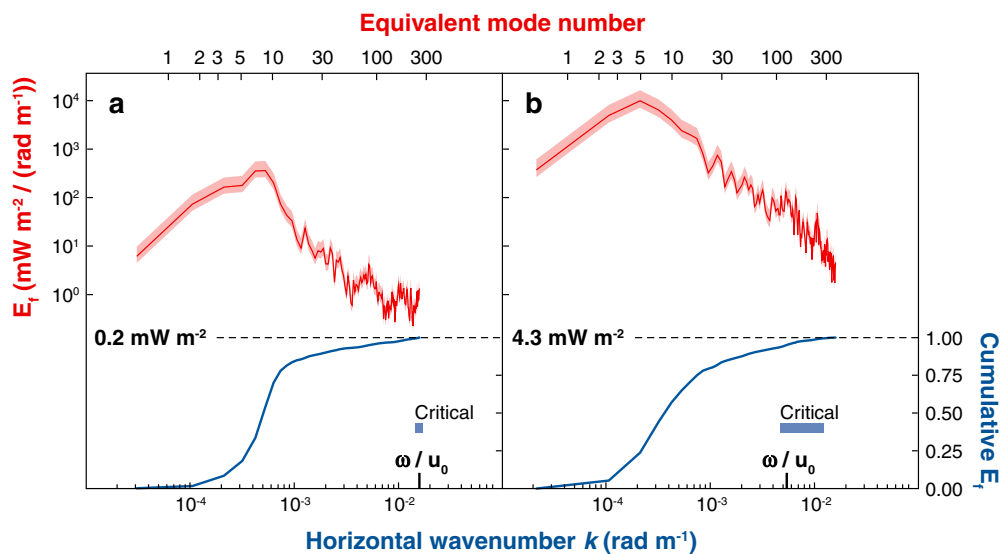


Figure 10

The energy flux into the M_2 internal tide at (a) the East Pacific Rise (EPR) and (b) the Mid-Atlantic Ridge (MAR) using the theory for small values of ϵ and ku_0/ω (red lines). The wavenumbers at which these parameters equal one are shown (“critical” corresponds to $\epsilon = 1$). The cumulative energy flux (as a fraction of the total) is also shown (blue lines), starting from a wavenumber corresponding to the lowest mode for the local ocean depth and stratification (St. Laurent & Garrett 2002).

flux is in low modes, for which the models are likely valid, rather than in high modes for which nonlinear terms may matter and the simple models are thus unreliable.

This is not to discount the high modes; they are likely to dominate local shears and local mixing. The point is that the overall oceanographic importance of internal tides may come from motions that are amenable to simple prediction schemes, at least as far as generation is concerned.

6.2. Numerical Models

A number of investigations of internal tide generation for particular oceanographic features have been conducted using layered models, even with just two layers, as this makes it easier to capture the effect of topographic variations in both horizontal directions with finite computational resources. For example, Kang et al. (2000) used a two-layer model to examine internal tide generation at the Hawaiian Ridge. The results show beams of internal tide energy originating from passages with strong barotropic flow. Horizontal beams have also been found in results from a model for the Aleutian Islands (Cummins et al. 2001).

The 3D nature of internal tide generation is also found in a model of the Hawaiian Ridge (Merrifield & Holloway 2002), with energy radiating from shallow saddles, between islands, with strong barotropic flow. As expected from simple models of abrupt topography, intense small-scale motions originate from places where the bottom slope is critical, but most of the energy flux is in low modes.

Although most numerical models of internal tide generation have been for specific features, Niwa & Hibiya (2001) evaluated the energy flux into internal tides for the whole Pacific Ocean by treating 17 subregions with a numerical model with $1/16^\circ$ horizontal resolution and 40 vertical levels. Their computed energy transfers from the barotropic to the internal tide agree reasonably well with Egbert & Ray's (2001) results, shown in **Figure 2**. As Cummins & Oey (1997) found for the region offshore of northern British Columbia, the generation of internal tide energy in specific regions is greater than that given by simple 2D (x, z) models, indicating the importance of 3D variations in the topography and barotropic currents.

Simmons et al. (2004) used a global model to estimate the energy flux into internal tides throughout the world's oceans. **Figure 11** shows the interface displacement, in a two-layer model with a mean interface depth of 1100 m, six days after the start of barotropic forcing.

The model shows radiation of internal tides from significant topographic features, with a wavelength proportional to $(\omega^2 - f^2)^{-1/2}$, as for the first mode, and therefore much shorter at low than at high latitudes. **Figure 11** also shows that the crests of the internal tide are not long, as would be the case for generation by a long, smooth ridge, but are more beam-like, corresponding to generation from different locations in ridges with varying height. Simmons et al. (2004) found that the energy flux into the internal tide does not change greatly when the ocean is represented by ten, instead of just two, layers, with a total flux of about 0.9 TW associated with M_2 . The flux appears to be dominated by the first mode, although model resolution did not permit reliable estimates of the flux into higher modes at low latitudes.

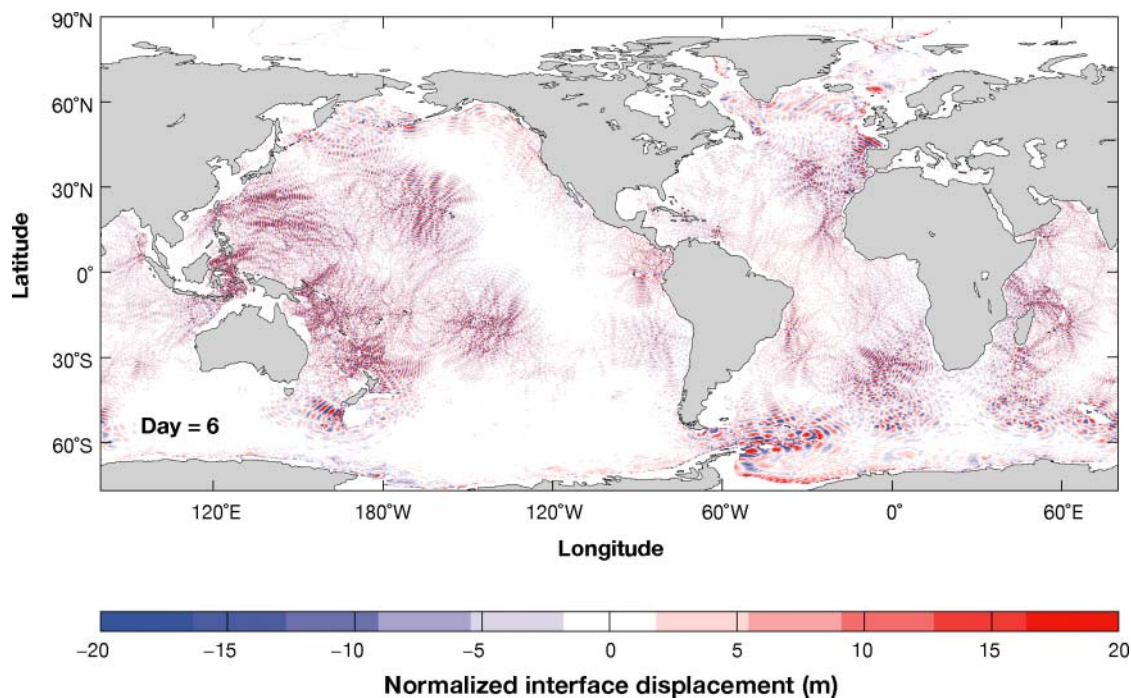


Figure 11

The interface displacement six days after the start of forcing, at the M_2 frequency, of a two-layer model (Simmons et al. 2004). The displacement has been adjusted to compensate for the use of horizontally uniform stratification.

These models generally include nonlinear terms, but they are so small that the model is effectively linear as far as the generation process is concerned. Model resolution does not allow a reliable evaluation of the complete cascade of the internal tide energy to smaller scales and turbulence, although the models can support predictions for the transfer of energy from the M_2 internal tide into half-frequency motions with a smaller vertical scale near 29° latitude, where the M_2 frequency is twice the inertial frequency (MacKinnon & Winters 2005, Simmons 2006), as strongly suggested by current meter data (Carter & Gregg 2006, Hibiya & Nagasawa 2006, van Haren 2005).

7. OCEANIC OBSERVATIONS

As stressed by Egbert & Ray (2001), the barotropic tides seem to be losing energy to internal tides in the deep sea at (a) gentle widespread bottom roughness associated with mid-ocean spreading centers such as the Mid-Atlantic Ridge (**Figure 2**), and (b) abrupt topography associated with island chains, ridges, and trenches. For the former, $\epsilon < 1$, at least for the scales responsible for most of the internal tide energy flux (**Figure 10**), and the height ratio $\delta \ll 1$, whereas for the latter the slope parameter

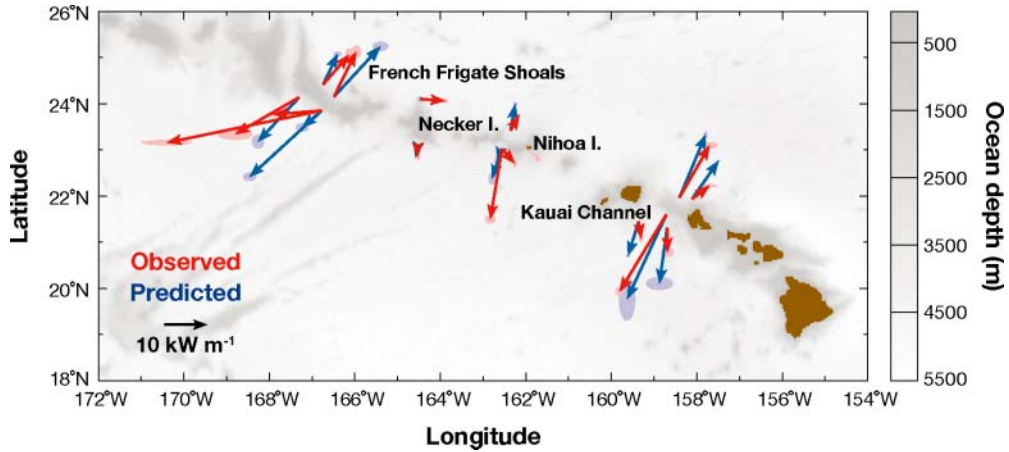


Figure 12

Observed (*red*) and predicted (*blue*) (Merrifield & Holloway 2002) vertically integrated horizontal energy fluxes from regions of the Hawaiian Ridge (Rudnick et al. 2003).

$\epsilon > 1$ and the height ratio $\delta = O(1)$. In both situations the excursion parameter ku_0/ω is small, except for the smallest scales of topography.

Although indirect evidence of internal tides has been found over gentle topography (**Figure 3**), direct in situ measurements of internal tide generation have thus far concentrated on abrupt topography. Field programs at Mendocino Escarpment (Althaus et al. 2003) and the Hawaiian Ridge (Lee et al. 2006, Martin et al. 2006, Nash et al. 2006, Rudnick et al. 2003) have confirmed many of the predictions from theories and numerical simulations. The observed magnitude of the energy flux radiated from sections of the Hawaiian Ridge agrees with model predictions to within a factor of 2 (**Figure 12**), although substantially larger than predicted along-ridge fluxes are observed (Lee et al. 2006). Fluxes vary by a factor of 10 along the ridge, indicating sensitivity to the varying ridge height and tidal flows.

A detailed investigation at Kaena Ridge, in the eastern part of Kauai Channel in **Figure 12**, shows two main beams of southward energy flux on the flank of the ridge (**Figure 13**). One is propagating upward and off the ridge in the upper 1000 m and seems to originate at the opposite side of the ridge crest at the transition from subcritical to supercritical slope. The other is propagating downward and off the ridge from the edge of the crest below 1200 m. There is no sign of a southward upward-propagating beam from the southern edge of the ridge crest.

A modal decomposition of the signals (**Figure 14**) shows that, in accord with theoretical expectations, much of the velocity signal (and hence energy) is in high modes, but the pressure, and hence the energy flux, are concentrated in low modes. The predominance of the energy flux in modes 1 and 2 is consistent with expectations for a knife edge or top hat (St. Laurent et al. 2003), and contrasts with the situation for the Mid-Atlantic Ridge shown in **Figure 10**, where the energy flux was spread mostly over modes 3 to about 10.

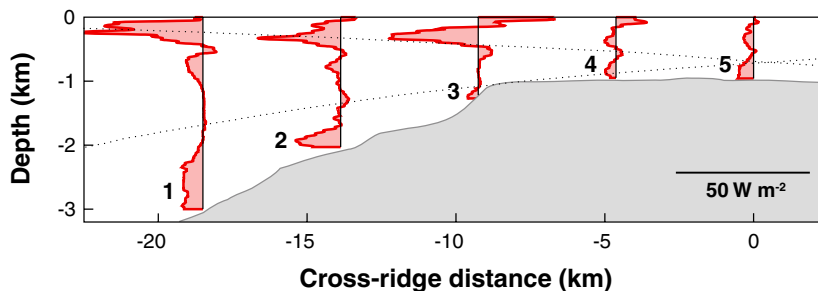


Figure 13
Cross-ridge energy flux profiles on the south side of Kaena Ridge, Hawaii (Nash et al. 2006). The dotted lines show the ray paths of the semidiurnal internal tide.

8. DISCUSSION AND OUTLOOK

The emphasis of this review has been on the fluid dynamics of internal tide generation. We have stressed the importance of organizing both problems and results in dimensionless parameter space, but have mainly addressed the parts of this space relevant to the deep ocean, rather than the typically different regime of shallow seas. In particular, it seems that radiated energy flux from large, steep, mid-ocean ridges

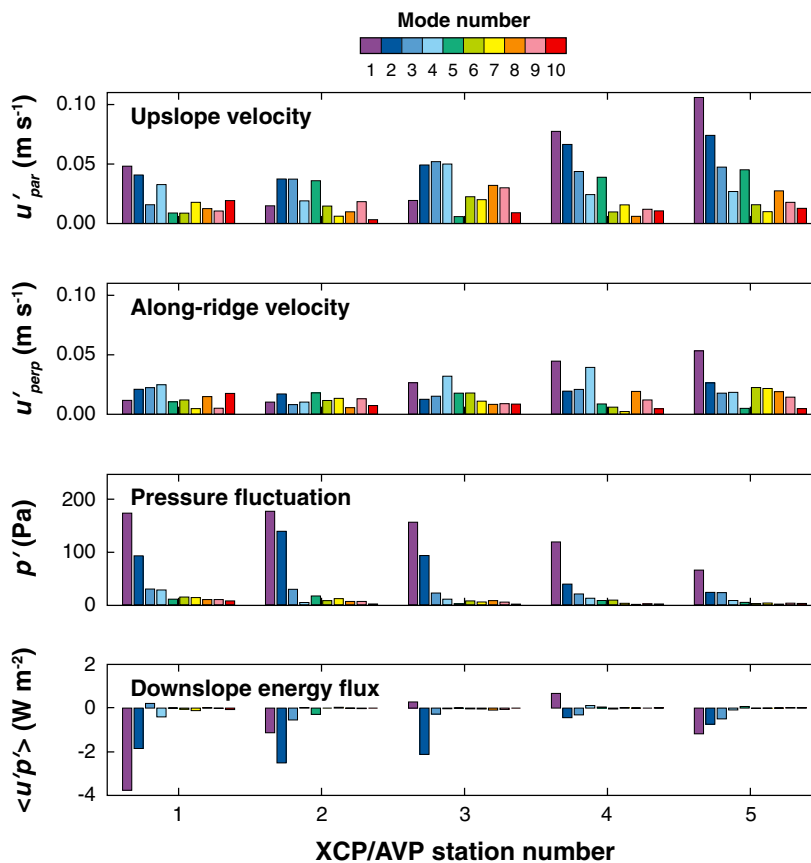


Figure 14
Modal decomposition of semidiurnal velocity, pressure, and energy flux for the first 10 flat-bottom modes in the profiles from **Figure 13** (Nash et al. 2006).

and island chains is dominated by low modes and is determined more by the height of topographic features than by details of the bottom slope. Regions of critical slope do act as sources of intense beams of internal tide energy, but contribute to the energy flux mostly by their mapping onto low modes. The high modes in the beam contribute little to the energy flux.

The fate of the radiated low modes is still uncertain. They may scatter into higher modes on further encounter with islands (Johnston et al. 2003, Johnston & Merrifield 2003) or the rough seafloor (St. Laurent & Garrett 2002), or transfer their energy to smaller-scale internal waves in the ocean interior (MacKinnon & Winters 2005, Polzin 2004, St. Laurent & Garrett 2002, van Haren 2005). Radiating beams can become nonlinear as they encounter strong near-surface stratification, leading directly to turbulence (Althaus et al. 2003) or breaking up into groups of higher frequency, short wavelength, nonlinear internal waves far from the original source (Gerkema 2001, New & da Silva 2002).

It does seem, though, that some of the internal tide energy flux from large topographic features in mid-ocean propagates across ocean basins to break on distant continental slopes (Nash et al. 2004). Thus, continental slopes may be significant sinks, rather than just sources, of internal tide energy! It is possible that dissipation on continental slopes partly occurs in homogenous boundary layers and is relatively inefficient at producing a vertical buoyancy flux, making internal tides less of a contributor to global ocean mixing than is sometimes assumed. This needs further investigation. The internal tides generated by the other class of deep-sea bottom topography, the rough regions of fracture zones, are in low-to-intermediate modes, and therefore more likely to cascade to turbulence in the open ocean, either by further bottom scattering or by nonlinear interactions in the ocean interior. Further discussion of the fate of internal tides is beyond the scope of this review.

The generation of internal tides still presents interesting fluid dynamical problems. In particular, it would be useful to extend to three dimensions the simple idealized analytical and numerical models that have led to useful conclusions in 2D situations. For a ridge of variable height, there might be enhanced generation at shallow parts of ridges (**Figure 6**), offset by a possible reduction of the barotropic current there as it is diverted to deeper parts of the ridge. Even for 2D problems, there are regions of the full dimensionless parameter space requiring further exploration.

ACKNOWLEDGMENTS

We are most grateful to colleagues who have provided figures, to Jennifer Kane for skillful contributions to the figures, and to Patrick Cummins, Theo Gerkema, Jody Klymak, Kevin Lamb, Walter Munk, Vasily Vlasenko, Carl Wunsch, and Bill Young for comments on a draft. We thank Canada's Natural Sciences and Engineering Research Council and the U.S. Office of Naval Research for support.

LITERATURE CITED

Althaus AM, Kunze E, Sanford TB. 2003. Internal tide radiation from Mendocino Escarpment. *J. Phys. Oceanogr.* 33:1510–27

- Baines PG. 1973. The generation of internal tides by flat-bump topography. *Deep-Sea Res.* 20:179–205
- Baines PG. 1982. On internal tide generation models. *Deep-Sea Res.* 29:307–38
- Baines PG. 1995. *Topographic Effects in Stratified Flows*. Cambridge, UK: Cambridge Univ. Press. 482 pp.
- Balmforth NJ, Ierley GR, Young WR. 2002. Tidal conversion by subcritical topography. *J. Phys. Oceanogr.* 32:2900–14
- Bell TH. 1975a. Lee waves in stratified flows with simple harmonic time dependence. *J. Fluid Mech.* 67:705–22
- Bell TH. 1975b. Topographically generated internal waves in the open ocean. *J. Geophys. Res.* 80:320–27
- Brink KH. 1990. On the generation of seamount-trapped waves. *Deep-Sea Res.* 37:1569–82
- Cacchione DA, Pratson LF, Ogston AS. 2002. The shaping of continental slopes by internal tides. *Science* 296:724–27
- Carter G, Gregg MC. 2006. Persistent near-diurnal internal waves observed above a site of M_2 barotropic-to-baroclinic conversion. *J. Phys. Oceanogr.* 36:1136–47
- Cartwright DE. 1999. *Tides: A Scientific History*. Cambridge, UK: Cambridge Univ. Press. 292 pp.
- Codiga DL, Eriksen CC. 1997. Observations of low-frequency circulation and amplified subinertial tidal currents at Cobb Seamount. *J. Geophys. Res.* 102:22993–3007
- Cox C, Sandstrom H. 1962. Coupling of internal and surface waves in water of variable depth. *J. Oceanogr. Soc. Jpn.* (20th Anniv. Vol.) 18:499–513
- Craig PD. 1987. Solution for internal tide generation over coastal topography. *J. Mar. Res.* 45:83–105
- Cummins PF, Armi L, Vagle S. 2006. Upstream internal hydraulic jumps. *J. Phys. Oceanogr.* 36:753–69
- Cummins PF, Cherniawsky JY, Foreman MG. 2001. North Pacific internal tides from the Aleutian Ridge: Altimeter observations and modeling. *J. Mar. Res.* 59:167–91
- Cummins PF, Oey L-Y. 1997. Simulation of barotropic and baroclinic tides off northern British Columbia. *J. Phys. Oceanogr.* 27:762–81
- Dushaw BD. 2006. Mode-1 internal tides in the western North Atlantic Ocean. *Deep-Sea Res. I* 53:449–73
- Egbert GD, Ray RD. 2000. Significant dissipation of tidal energy in the deep ocean inferred from satellite altimeter data. *Nature* 405:775–78
- Egbert GD, Ray RD. 2001. Estimates of M_2 tidal dissipation from TOPEX/Poseidon altimeter data. *J. Geophys. Res.* 106:22475–502
- Farmer DM, Freeland HJ. 1983. The physical oceanography of fjords. *Prog. Oceanogr.* 12:147–200
- Farmer DM, Smith JD. 1980. Tidal interactions of stratified flow with a sill in Knight Inlet. *Deep-Sea Res.* 27A:239–54
- Farmer D, Armi L. 1999. The generation and trapping of solitary waves over topography. *Science* 283:188–90
- Garrett C. 1979. Mixing in the ocean interior. *Dyn. Atmos. Oceans* 3:239–65

- Garrett C. 2003. Internal tides and ocean mixing. *Science* 301:1858–59
- Garrett C, Gerkema T. 2006. A note on the bodyforce term in internal-tide generation. *J. Phys. Oceanogr.* In press
- Gerkema T. 1996. A unified model for the generation and fission of internal tides in a rotating ocean. *J. Mar. Res.* 54:421–50
- Gerkema T. 2001. Internal and interfacial tides: Beam scattering and local generation of solitary waves. *J. Mar. Res.* 59:227–55
- Gerkema T, Lam F-PA, Maas LRM. 2004. Internal tides in the Bay of Biscay: conversion rates and seasonal effects. *Deep-Sea Res. II* 51:2995–3008
- Gerkema T, Zimmerman JTF. 1995. Generation of nonlinear internal tides and solitary waves. *J. Phys. Oceanogr.* 25:1081–1094
- Gill AE. 1982. *Atmosphere-Ocean Dynamics*. New York: Academic. 662 pp.
- Haurly LR, Briscoe MG, Orr MH. 1979. Tidally generated internal wave packets in Massachusetts Bay. *Nature* 278:312–17
- Hendershott M. 1981. Long waves and ocean tides. In *Evolution of Physical Oceanography*, ed. BA Warren, C Wunsch, pp. 292–341. Cambridge, MA: MIT Press
- Heney FS, Hoering A. 1997. Energetics of borelike internal waves. *J. Geophys. Res.* 102:3323–30
- Hibiya T. 1986. Generation mechanism of internal waves by tidal flow over a sill. *J. Geophys. Res.* 91:7697–708
- Hibiya T. 1988. The generation of internal waves by tidal flow over Stellwagen Bank. *J. Geophys. Res.* 93:533–42
- Hibiya T, Nagasawa M. 2004. Latitudinal dependence of diapycnal diffusivity in the thermocline estimated using a finescale parameterization. *Geophys. Res. Lett.* 31:L01301, doi: 10.1029/2003GL017998
- Holloway PE. 1987. Internal hydraulic jumps and solitons at a shelf break region on the Australian North West Shelf. *J. Geophys. Res.* 92:5405–16
- Holloway PE. 1996. A numerical model of internal tides with application to the Australian North West Shelf. *J. Phys. Oceanogr.* 26:212–37
- Holloway PE, Merrifield MA. 1999. Internal tide generation by seamounts, ridges, and islands. *J. Geophys. Res.* 104:25937–51
- Holloway PE, Pelinovsky EP, Talipova T, Barnes B. 1997. A nonlinear model of internal tide transformation on the Australian North-West shelf. *J. Phys. Oceanogr.* 27:871–96
- Hurley DG. 1997. The generation of internal waves by vibrating elliptic cylinders. Part 1. Inviscid solution. *J. Fluid Mech.* 351:105–18
- Johnston TMS, Merrifield MA. 2003. Internal tide scattering at seamounts, ridges, and islands. *J. Geophys. Res.* 108(C6):3180
- Johnston TMS, Merrifield MA, Holloway PE. 2003. Internal tide scattering at the Line Islands Ridge. *J. Geophys. Res.* 108(C11):3365
- Kang S-K, Foreman M, Crawford W, Cherniawsky J. 2000. Numerical modeling of internal tide generation along the Hawaiian ridge. *J. Phys. Oceanogr.* 30:1083–98
- Kantha LH, Tierney CC. 1997. Global baroclinic tides. *Prog. Oceanogr.* 40:163–78
- Khatiwala S. 2003. Generation of internal tides in an ocean of finite depth: analytical and numerical calculations. *Deep-Sea Res. I* 50:3–21

- Klymak JM, Gregg MC. 2004. Tidally generated turbulence over the Knight Inlet sill. *J. Phys. Oceanogr.* 34:1135–51
- Lamb KG. 1994. Numerical experiments of internal wave generation by strong tidal flow across a finite amplitude bank edge. *J. Geophys. Res.* 99:843–64
- Ledwell JR, Montgomery ET, Polzin KL, St. Laurent LC, Schmitt RW, Toole JM. 2000. Evidence for enhanced mixing over rough topography in the abyssal ocean. *Nature* 403:179–82
- Lee CM, Kunze E, Sanford TB, Nash JD, Merrifield MA, Holloway PE. 2006. Internal tides and turbulence along the 3000-m isobath of the Hawaiian Ridge. *J. Phys. Oceanogr.* 36:1165–83
- Legg S. 2004a. Internal tides generated on a corrugated continental slope. Part I: Cross-slope barotropic forcing. *J. Phys. Oceanogr.* 34:156–73
- Legg S. 2004b. Internal tides generated on a corrugated continental slope. Part II: Along-slope barotropic forcing. *J. Phys. Oceanogr.* 34:1824–38
- Legg S, Huijts KMH. 2006. Preliminary simulations of internal waves and mixing generated by finite amplitude tidal flow over isolated topography. *Deep-Sea Res. II* 53:140–56
- Llewellyn Smith SG, Young WR. 2002. Conversion of the barotropic tide. *J. Phys. Oceanogr.* 32:1554–66
- Llewellyn Smith SG, Young WR. 2003. Tidal conversion at a very steep ridge. *J. Fluid Mech.* 495:175–91
- MacKinnon JA, Winters KB. 2006. Tidal mixing hotspots governed by rapid parametric subharmonic instability. *J. Phys. Oceanogr.* Submitted
- Martin JP, Rudnick DL, Pinkel R. 2006. Spatially-broad observations of internal waves in the upper ocean at the Hawaiian Ridge. *J. Phys. Oceanogr.* 36:1085–103
- Matsuura T, Hibiya T. 1990. An experimental and numerical study of the internal wave generation by tide–topography interaction. *J. Phys. Oceanogr.* 20:506–21
- McPhee-Shaw E. 2006. Boundary-interior exchange. Reviewing the idea that internal-wave mixing enhances lateral dispersal near continental margins. *Deep-Sea Res. II* 53:42–59
- Merrifield MA, Holloway PE. 2002. Model estimates of M_2 internal tide energetics at the Hawaiian Ridge. *J. Geophys. Res.* 107(C8):3179
- Morozov EG. 1995. Semidiurnal internal wave global field. *Deep-Sea Res.* 42:135–48
- Munk W, Wunsch C. 1998. Abyssal recipes II: energetics of tidal and wind mixing. *Deep-Sea Res.* 45:1977–2010
- Munroe JR, Lamb KG. 2005. Topographic amplitude dependence of internal wave generation by tidal forcing over idealized three-dimensional topography. *J. Geophys. Res.* 110(C2):CO2001
- Nakamura T, Awaji T, Hatayama T, Akitomo K, Takizawa T, et al. 2000. The generation of large-amplitude unsteady lee waves by subinertial K_1 tidal flow: A possible vertical mixing mechanism in the Kuril Straits. *J. Phys. Oceanogr.* 30:1601–21
- Nansen F. 1902. *Oceanography of the North Pole Basin: Norwegian North Polar Expedition, 1893–1896. Scientific Results*, 3(9):1–427
- Nash JD, Kunze E, Lee CM, Sanford TB. 2006. Structure of the baroclinic tide generated at Kaena Ridge, Hawaii. *J. Phys. Oceanogr.* 36:1123–35

- Nash JD, Kunze E, Toole JM, Schmitt RW. 2004. Internal tide reflection and turbulent mixing on the continental slope. *J. Phys. Oceanogr.* 34:1117-34
- New AL, da Silva JCB. 2002. Remote-sensing evidence for the local generation of internal soliton packets in the central Bay of Biscay. *Deep-Sea Res. I* 49:915-34
- Niwa Y, Hibiya T. 2001. Numerical study of the spatial distribution of the M_2 internal tide in the Pacific Ocean. *J. Geophys. Res.* 106:22441-49
- Osborne AR, Burch TL. 1980. Internal solitons in the Andaman Sea. *Science* 208:451-60
- Osborne AR, Burch TL, Scarlet RI. 1978. The influence of internal waves on deep-water drilling. *J. Pet. Technol.* 30:1497-1504
- Pétréris F, Llewellyn Smith SG, Young WR. 2006. Tidal conversion at a submarine ridge. *J. Phys. Oceanogr.* 36:1053-71
- Pettersson O. 1908. Strömstudier vid Östersjönsportar. *Sven. Hydrogr. Biol. Komm. Skr.* 3:13-37
- Pingree RD, Mardell GT. 1985. Solitary internal waves in the Celtic Sea. *Prog. Oceanogr.* 14:431-41
- Pingree RD, Mardell GT, New AL. 1986. Propagation of internal tides from the upper slopes of the Bay of Biscay. *Nature* 321:154-58
- Polzin K. 2004. Idealized solutions for the energy balance of the finescale internal wave field. *J. Phys. Oceanogr.* 34:231-46
- Prinsenbergh SJ, Rattray M Jr. 1975. Effects of continental slope and variable Brunt-Väisälä frequency on the coastal generation of internal tides. *Deep-Sea Res.* 22:251-65
- Radko T, Marshall J. 2004. Eddy-induced diapycnal fluxes and their role in the maintenance of the thermocline. *J. Phys. Oceanogr.* 34:372-83
- Rattray M. 1960. On the coastal generation of internal tides. *Tellus* 12:54-62
- Ray RD, Mitchum GT. 1997. Surface manifestations of internal tides in the deep ocean: observations from altimetry and island gauges. *Prog. Oceanogr.* 40:135-62
- Rippeth TP, Inall ME. 2002. Observations of the internal tide and associated mixing across the Malin Shelf. *J. Geophys. Res.* 107(C4):3028
- Robinson RM. 1969. The effects of a vertical barrier on internal waves. *Deep-Sea Res.* 16:421-29
- Rudnick DL, Boyd TJ, Brainard RE, Carter GS, Egbert GD, et al. 2003. From tides to mixing along the Hawaiian Ridge. *Science* 301:355-57
- Samelson RM. 1998. Large-scale circulation with locally enhanced vertical mixing. *J. Phys. Oceanogr.* 28:712-26
- Sandstrom H, Elliott JA. 1984. Internal tide and solitons on the Scotian Shelf: A nutrient pump at work. *J. Geophys. Res.* 89:6415-26
- Schott F. 1977. On the energetics of baroclinic tides in the North Atlantic. *Ann. Géophys.* 33:41-62
- Simmons HL. 2006. The geography of subharmonic instability of the semi-diurnal internal tide. *J. Phys. Oceanogr.* Submitted
- Simmons HL, Hallberg RW, Arbic BK. 2004. Internal wave generation in a global baroclinic tidal model. *Deep-Sea Res. II* 51:3043-68

- Smith WHF, Sandwell DT. 1997. Global seafloor topography from satellite altimetry and ship depth soundings. *Science* 277:1956–62
- St. Laurent L, Garrett C. 2002. The role of internal tides in mixing the deep ocean. *J. Phys. Oceanogr.* 32:2882–99
- St. Laurent L, Stringer S, Garrett C, Perrault-Joncas D. 2003. The generation of internal tides at abrupt topography. *Deep-Sea Res. I* 50:987–1003
- Toole JM, Ledwell JR, Polzin KL, Schmitt RW, Montgomery ET, et al. 1997. The Brazil Basin Tracer Release Experiment. *Int. WOCE Newsl.* 28:25–28
- van Haren H. 2005. Tidal and near-inertial peak variations around the diurnal critical latitude. *Geophys. Res. Lett.* 32(23):L23611
- Vlasenko V, Ivanov VA, Krasin IG, Lisichenok AD. 1996. Study of intensive internal waves in the shelf zone of Morocco. *Phys. Oceanogr.* 7:281–98
- Vlasenko V, Stashchuk N, Hutter K. 2005. *Baroclinic Tides: Theoretical Modeling and Observational Evidence*. Cambridge, UK: Cambridge Univ. Press. 351 pp.
- Wunsch C. 1975. Internal tides in the ocean. *Rev. Geophys. Space Phys.* 13:167–82
- Wunsch C, Ferrari R. 2004. Vertical mixing, energy, and the general circulation of the oceans. *Annu. Rev. Fluid Mech.* 36:281–314
- Zeilon N. 1912. On tidal boundary-waves and related hydrodynamical problems. *Kungliga Sven. Vetensk. Handl. Ny Följden* 47(4):1–46
- Zeilon N. 1934. Experiments on boundary tides. A preliminary report. *Göteborg. Kungliga Vetensk. Vitterh.-Samb. Handl., Femten Följden, Ser. B* 3(10):1–8
- Zhang J, Schmitt RW, Huang RX. 1999. The relative influence of diapycnal mixing and hydrological forcing on the stability of the thermohaline circulation. *J. Phys. Oceanogr.* 29:1096–108



Contents

H. Julian Allen: An Appreciation <i>Walter G. Vincenti, John W. Boyd, and Glenn E. Bugos</i>	1
Osborne Reynolds and the Publication of His Papers on Turbulent Flow <i>Derek Jackson and Brian Launder</i>	18
Hydrodynamics of Coral Reefs <i>Stephen G. Monismith</i>	37
Internal Tide Generation in the Deep Ocean <i>Chris Garrett and Eric Kunze</i>	57
Micro- and Nanoparticles via Capillary Flows <i>Antonio Barrero and Ignacio G. Loscertales</i>	89
Transition Beneath Vortical Disturbances <i>Paul Durbin and Xiaohua Wu</i>	107
Nonmodal Stability Theory <i>Peter J. Schmid</i>	129
Intrinsic Flame Instabilities in Premixed and Nonpremixed Combustion <i>Moshe Matalon</i>	163
Thermofluid Modeling of Fuel Cells <i>John B. Young</i>	193
The Fluid Dynamics of Taylor Cones <i>Juan Fernández de la Mora</i>	217
Gravity Current Interaction with Interfaces <i>J. J. Monaghan</i>	245
The Dynamics of Detonation in Explosive Systems <i>John B. Bdzil and D. Scott Stewart</i>	263
The Biomechanics of Arterial Aneurysms <i>Juan C. Lasheras</i>	293

The Fluid Mechanics Inside a Volcano <i>Helge M. Gonnemann and Michael Manga</i>	321
Stented Artery Flow Patterns and Their Effects on the Artery Wall <i>Nandini Duraiswamy, Richard T. Schoephoerster, Michael R. Moreno, and James E. Moore, Jr.</i>	357
A Linear Systems Approach to Flow Control <i>John Kim and Thomas R. Bewley</i>	383
Fragmentation <i>E. Villermaux</i>	419
Turbulence Transition in Pipe Flow <i>Bruno Eckhardt, Tobias M. Schneider, Bjorn Hof, and Jerry Westerweel</i>	447
Waterbells and Liquid Sheets <i>Christophe Clanet</i>	469

Indexes

Subject Index	497
Cumulative Index of Contributing Authors, Volumes 1–39	511
Cumulative Index of Chapter Titles, Volumes 1–39	518

Errata

An online log of corrections to *Annual Review of Fluid Mechanics* chapters (1997 to the present) may be found at <http://fluid.annualreviews.org/errata.shtml>